Cell Reports

Article

Developmental Alterations in Heart Biomechanics and Skeletal Muscle Function in Desmin Mutants Suggest an Early Pathological Root for Desminopathies

Graphical Abstract

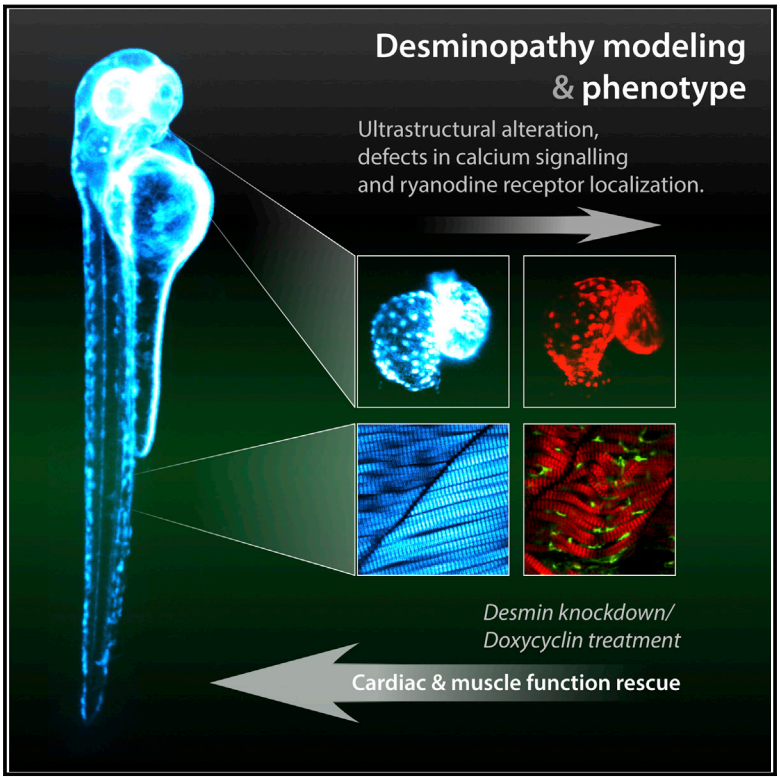

Highlights

- A knockin in the *Desmin* gene allows in vivo imaging of Desmin aggregates
- Knockout and knockin of Desmin alters skeletal muscle and cardiomyocyte function
- Excitation-contraction coupling is affected in Desmin knockout and knockin
- Doxycycline and decreased Desmin expression rescue muscle and cardiac function

Authors

Caroline Ramspacher, Emily Steed, Francesco Boselli, ..., Jocelyn Laporte, Karim Hnia, Julien Vermot

Correspondence

julien@igbmc.fr

In Brief

Desminopathies are myopathies and cardiomyopathies associated with Desmin mutations leading to protein aggregates. Ramspacher et al. demonstrate that altered Desmin function or expression affect the EC coupling machinery and calcium dynamics. They show that aggregates are more toxic than the loss of function and can be rescued by knockdown and pharmacological treatment.

Ramspacher et al., 2015, Cell Reports *11*, 1564–1576
June 16, 2015 ©2015 The Authors
http://dx.doi.org/10.1016/j.celrep.2015.05.010

CrossMark

CellPress

OPEN ACCESS
CellPress

Cell Reports
Article

Developmental Alterations in Heart Biomechanics and Skeletal Muscle Function in Desmin Mutants Suggest an Early Pathological Root for Desminopathies

Caroline Ramspacher,[1,2,3,4] Emily Steed,[1,2,3,4] Francesco Boselli,[1,2,3,4] Rita Ferreira,[1,2,3,4] Nathalie Faggianelli,[1,2,3,4] Stéphane Roth,[1,2,3,4] Coralie Spiegelhalter,[1,2,3,4] Nadia Messaddeq,[1,2,3,4] Le Trinh,[5] Michael Liebling,[6] Nikhil Chacko,[6] Federico Tessadori,[7] Jeroen Bakkers,[7] Jocelyn Laporte,[1,2,3,4] Karim Hnia,[1,2,3,4] and Julien Vermot[1,2,3,4,*]

[1]Institut de Génétique et de Biologie Moléculaire et Cellulaire, 67404 Illkirch, France
[2]Centre National de la Recherche Scientifique, UMR7104, 67404 Illkirch, France
[3]Institut National de la Santé et de la Recherche Médicale, U964, 67404 Illkirch, France
[4]Université de Strasbourg, 67404 Illkirch, France
[5]Molecular and Computational Biology, University of Southern California, Los Angeles, CA 90089, USA
[6]Department of Electrical and Computer Engineering, University of California Santa Barbara, Santa Barbara, CA 93106, USA
[7]Hubrecht Institute-KNAW and University Medical Center Utrecht, Utrecht 3584 CT, the Netherlands
*Correspondence: julien@igbmc.fr
http://dx.doi.org/10.1016/j.celrep.2015.05.010
This is an open access article under the CC BY-NC-ND license (http://creativecommons.org/licenses/by-nc-nd/4.0/).

SUMMARY

Desminopathies belong to a family of muscle disorders called myofibrillar myopathies that are caused by Desmin mutations and lead to protein aggregates in muscle fibers. To date, the initial pathological steps of desminopathies and the impact of desmin aggregates in the genesis of the disease are unclear. Using live, high-resolution microscopy, we show that Desmin loss of function and Desmin aggregates promote skeletal muscle defects and alter heart biomechanics. In addition, we show that the calcium dynamics associated with heart contraction are impaired and are associated with sarcoplasmic reticulum dilatation as well as abnormal subcellular distribution of Ryanodine receptors. Our results demonstrate that desminopathies are associated with perturbed excitation-contraction coupling machinery and that aggregates are more detrimental than Desmin loss of function. Additionally, we show that pharmacological inhibition of aggregate formation and Desmin knockdown revert these phenotypes. Our data suggest alternative therapeutic approaches and further our understanding of the molecular determinants modulating Desmin aggregate formation.

INTRODUCTION

Proteinopathies form a group of diseases with well-recognized features mainly hallmarked by protein aggregation. Desminopathies belong to the myofibrillar myopathies and comprise primary Desmin Related Myopathy and Cardiomyopathy (DRM and DRCM). Both DRM and DRCM are characterized by intracellular accumulation of misfolded proteins and the presence of desmin-positive insoluble granulofilamentous aggregates. Desmin-related diseases lead to progressive skeletal muscle weakness, cardiomyopathy, and conduction defects (van Spaendonck-Zwarts et al., 2011). The first symptoms of desminopathies in humans generally occur in the third decade, but the disease onset and the rate of progression of desminopathies are highly variable. Interestingly, numerous muscular disorders have been characterized as secondary DRM by the presence of desmin aggregates (Griggs et al., 2007; Hnia et al., 2011). The kinetics of aggregate formation in vivo remains unclear, and the contribution of these aggregates to developmental defects is still unknown. Thus, developing a model organism in which aggregate formation can be visualized in vivo will help elucidate the developmental defects underlying desminopathies and understand the dynamics of desmin aggregation and its impact on muscle function during embryogenesis.

Desmin is a muscle-specific type III intermediate filament protein essential for proper muscular function (Li et al., 1996; Milner et al., 1996). Mutations affecting desmin function or promoting desmin aggregation can promote skeletal or cardiac muscle phenotypes or both. Desmin knockout (KO) mice (Li et al., 1996; Milner et al., 1996) exhibit a loss of lateral alignment of myofibrils from the second week after birth. This phenotype is more severe in the heart and leads to progressive degeneration, calcification, and necrosis of the myocardium. Desmin was proposed to act as a scaffolding protein providing viscoelastic properties in the vascular wall (Lacolley et al., 2001) and stiffness to myocytes (Anderson et al., 2001), the lung airways (Shardonofsky et al., 2006), as well as the cardiomyocytes (Balogh et al., 2002; Costa et al., 2004; Rezniczek et al., 2007). The embryonic heart pumping is dependent on the biomechanical properties of cardiomyocytes (Forouhar et al., 2006), yet the role of desmin on heart biomechanics in vivo remains largely unexplored. Therefore, addressing whether there are mechanical mechanisms associated with desmin function that influence heart pumping and whether desmin aggregates affect these biomechanical mechanisms would help to solve this issue. To date, several mouse models of

desmin-related myopathy, consisting of knockin mice carrying specific patient's point mutations, were generated, yet most of them did not present clear aggregate structures, and subsequent phenotypes were often associated to dominant-negative effects on the desmin network rather than to aggregate formation (Joanne et al., 2013; Kostareva et al., 2008; Raats et al., 1996). So far, desmin aggregation was observed in mouse cardiomyocytes carrying a specific desmin mutation (Wang et al., 2001a) or *CRYAB* mutation (Wang et al., 2001b). Similarly, morpholino (MO)-mediated knockdown in zebrafish leads to cardiac and skeletal muscle phenotype (Li et al., 2013; Vogel et al., 2009). Yet, the role of desmin in heart function is still not well known, but it has been suggested that desmin impacts the mechanical properties of the cardiomyocytes (Hnia et al., 2014). Nevertheless, the sequence of events leading to these cellular alterations and their temporal relationship with protein aggregation have not yet been investigated. Thus, a comparison between desmin loss of function and pathological desmin aggregation would help to identify the cellular defects associated with either desmin depletion or aggregate formation alone.

In this study, we used genetically engineered zebrafish models allowing the comparative study of the effect of desmin aggregate formation and desmin loss of function to answer these questions. We found that desmin loss of function and the formation of desmin aggregates participate in multiple defects affecting skeletal and cardiac muscles, as well as vascular development and function in the zebrafish larvae. These defects are associated with abnormal calcium flux due to the disruption of excitation-contraction (EC) coupling machinery and to an abnormal subcellular localization of Ryanodine receptor (RyR) in both types of mutants. We further demonstrated that the majority of pathological phenotypes could be rescued by doxycycline treatment or desmin knockdown (MO), which could be of high interest for future treatment of desminopathies. Altogether, our results identify Desmin as an essential element in controlling embryonic cardiovascular and skeletal muscle function, due to its role in controlling myocardial cell contractile properties and calcium signaling. Furthermore, despite desmin being essential for heart function, its reduction is beneficial when aggregates are present and represents a potential therapeutic approach for patients.

RESULTS

Generation and Characterization of the *desma* Citrine (*desma*^{Ct122aGt}) and *desma* mCherry (*desma*^{Ct122aRGt}) Zebrafish Lines

Desmin intermediate filaments polymerize to form polymers following gradual steps of the classical assembly of intermediate filaments (Herrmann et al., 2009). The zebrafish *desmin a* (*desma*) gene is homologous to human desmin with 81% similarity in the protein sequences. *desmin b (desmb)*, a second homolog of human Desmin sharing 83% similarity, also exists in zebrafish (Figure S1). qPCR experiments and in situ hybridization showed that the expression level of *desmb* is low at early times of development (around 2,500-fold lower than the level of *desma* in 48 hpf wild-type embryos), and no overexpression of *desmb* was observed upon *desma* depletion (Figure S1). Accordingly, we conclude that the uncovered desmin protein distribution is reminiscent of Desma and that the expression of *desmb* can be neglected before 96 hpf.

Several desmin mutations have been shown to interfere with proper filament assembly when tested in vitro (Bär et al., 2005a, 2010). Such mutations could also promote aggregate formation when transfected into cultured cells (Bär et al., 2005b). However, these observations are at the steady-state level and do not provide information on aggregate formation and dynamics. In order to address the role of desmin aggregates in vivo, we used a knockin line where citrine has been inserted between amino acids 460 and 461 in the C terminus of *desmin a.* This line, named *desma*^{Ct122aGt} (or *ct122aGt*), was obtained from a gene trap screen. In this genetic context, the *desma* gene contains an artificial exon intercalating the citrine fluorescent protein coding sequence within the gene. This method enables in vivo expression of labeled Desmin at endogenous levels (Trinh et al., 2011). For the second line, we made use of the FlipTrap capability in the *desma*^{ct122aGt} line to undergo Cre-lox recombination. Upon Cre-lox recombination, the *desma*^{ct122aGt} is converted to a mCherry fusion that truncates the Desma protein, leading to a mCherry tag followed by a stop codon in the case of the reverted *desma*^{Ct122aRGt} (or *ct122aRGt*) line, leading to the deletion of 13 C-terminal amino acids in the tail domain (Figure 1A). We analyzed the global shape of the embryo and larvae as well as the viability of the *ct122aGt* and found they display no overall defects and develop normally (Figure 1B). The insertion of the fluorescent tag leads to Desmin aggregation in both lines in myocardial and skeletal muscles at 48 hpf (Figures 1C and 1D). Correlative light and electron microscopy (CLEM) using tomography showed that *ct122aGt* aggregates are positioned throughout the cytoplasm and have a fibrous structure and an average size of 9.7 ± 0.4 μm at 48 hpf (Figures 1E and 1F; Movie S1). We segmented the aggregates in 3D, and analysis of the reconstructions shows that the core structure of the aggregates is a cluster of Desmin filaments packed into a disorganized network (Movie S1).

Similar to *ct122aGt*, aggregates were observed both in the heart and skeletal muscles in the *ct122aRGt* line. Subsequent analysis of the Desma aggregate size and structure revealed that *ct122aRGt* aggregates are positioned throughout the cytoplasm similarly to what is observed in *ct122aGt*, but they are more electron dense and have a more granular structure than the *ct122aGt* aggregates (Figure 1E). Their average size was also smaller (1.4 ± 0.05 μm). In the myocardium, these aggregates were found preferentially close to cardiomyocyte membranes (Figure S1G). The differences observed between the *ct122aGt* and *ct122aRGt* lines suggest that Desma aggregation properties depend on its sequence integrity. This highlights the heterogeneity of aggregate size and shape reminiscent of *desmin* mutations, which is also observed in different human mutations (Bär et al., 2005b; Brodehl et al., 2012).

Desmin Loss or Aggregation Leads to Muscle Disorganization and Altered Organelles

Desminopathies are characterized by accumulation of granulofilamentous material leading to progressive muscle weakness with specific histological hallmarks, such as misshaped and mislocalized mitochondria, z-band streaming, and myofibrillar

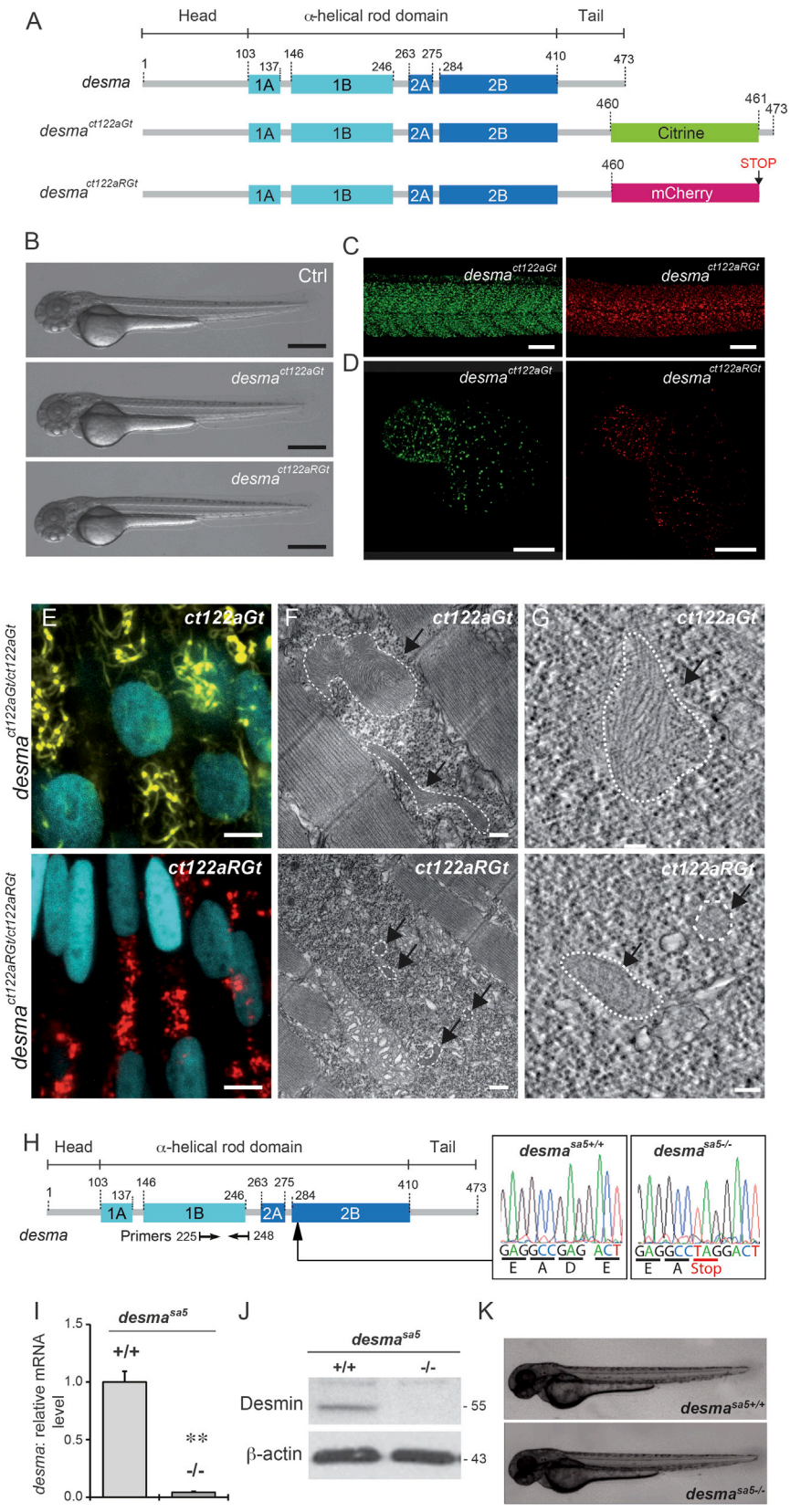

Figure 1. Desmin Flip Trap Fish Lines, *desma*^{ct122aGt} and *desma*^{ct122aRGt}, Enable Formation and Visualization of Desmin Aggregates while the *desma*$^{sa5-/-}$ Allele Leads to a Loss of *desma* Transcripts

(A) Schematic drawing of the *desma* gene in WT, *desma*^{ct122aGt} or *ct122aGt* (with citrine fusion), and *desma*^{ct122aRGt} or *Ct122aRGt* (with mCherry fusion) fish lines. The *ct122aRGt* line presents a 13-amino-acid deletion at the end of the tail domain, and the *ct122aGt* line presents a full *desma* sequence containing the citrine fluorescent protein.

(B) Side views of *ct122aGt* and *ct122aRGt* zebrafish embryos at 55 hpf. Scale bar, 500 μm.

(C and D) Desmin aggregates are observed in skeletal muscles (scale bar, 100 μm) (C) and in the myocardium (scale bar, 50 μm) (D) in *ct122aGt* and *ct122aRGt* 48-hpf embryos.

(E–G) Semicorrelative light and electron microscopy of skeletal muscles of *ct122aGt* and *ct122aRGt* 48-hpf embryos. (E) Confocal micrograph at high magnification of ct122aGt and *ct122aRGt* embryos. Nuclei are labeled with H2B-Cerulean. Scale bar, 5 μm. (F) Electron micrograph analyses of the same region showed cytosolic aggregates (the black arrows are pointing to the aggregates circled by the dotted lines) in *ct122aGt* and *ct122aRGt* embryos. Scale bar, 200 nm. (G) Electron tomography at high magnification showing filamentous aggregate structures in ct122aGt and compact aggregates with regular condensed structure in the *ct122aRGt* (the black arrows are pointing to the aggregates circled by the dotted lines). Scale bar, 100 nm. *ct122aGt* and *ct122aRGt* refers to homozygous embryos.

(H) Scheme of the WT *desma* gene in zebrafish. Arrow indicates the position of the mutation in the *desma* gene sequence. Sequencing of genomic DNA from *desma*$^{sa5+/+}$ and *desma*$^{sa5-/-}$ larvae reveals a G to T mutation resulting in a stop codon that leads to truncated Desma in *desma*$^{sa5-/-}$ mutants.

(I) Reverse transcriptase qPCR on RNA extracted from pools of WT and *desma*$^{sa5-/-}$ mutants demonstrates defective amplification of the mutant transcripts of exons 3–4 demonstrating that the corresponding mRNA is degraded. The primers used for qPCR are highlighted in (A).

(J) Immunoblot of 2 dpf WT and *desma*$^{sa5-/-}$ mutants demonstrating full knockdown of Desma protein.

(K) Side views of zebrafish *desma*$^{sa5+/+}$ and *desma*$^{sa5-/-}$ embryos at 55 hpf.

Scale bar, 500 μm. The error bars correspond to the SEM.

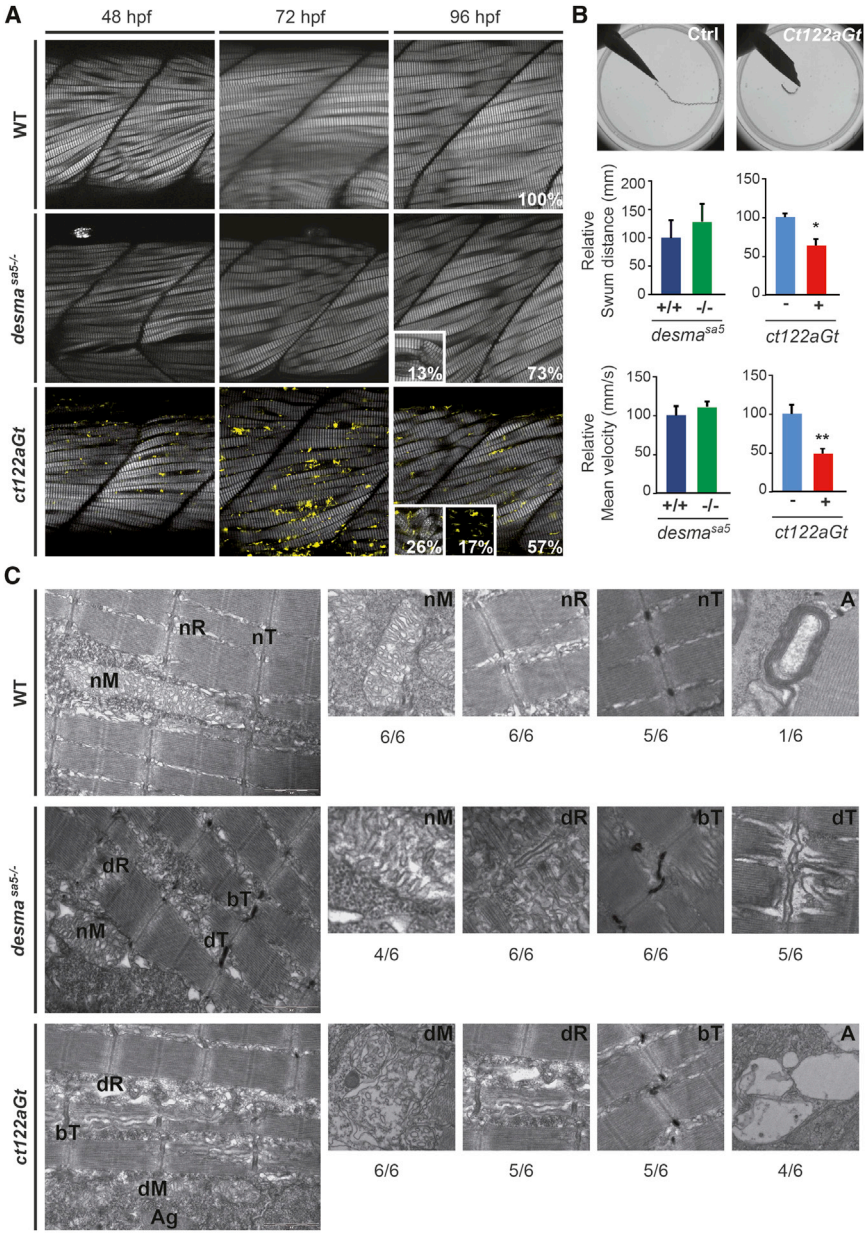

Figure 2. Aggravation of the Skeletal Muscle Phenotype Is Observed in *desma*^{ct122aGt} Embryos Compared to *desma*$^{sa5-/-}$

(A) Optical sections of the mid trunk region using SHG imaging show misalignment of muscle fibers in *desma*$^{sa5-/-}$ and *desma*^{ct122aGt} homozygous embryos compared to WT siblings at 48, 72, and 96 hpf. In *ct122aGt* mutants, muscle fiber misalignment is often accompanied by fiber breaks and degeneration from 48 hpf. At 96 hpf, phenotypes are separated in to three categories: weak *(W)* with misalignment only; strong *(S)* (see inset at 96 hpf for the *desma*^{ct122aGt} and *desma*$^{sa5-/-}$) with misalignment accompanied with breaks, degenerations, and/or general decrease of the SHG intensity; and extreme *(E)* (see inset at 96 hpf for the *desma*^{ct122aGt}) where the SHG signal is absent because of the complete disorganization of sarcomeric structures. Scale bar, 20 μm.

(B) Touch-evoke response assays show reduced swimming distance and velocity in *ct122aGt* embryos compared to controls, while the locomotion capacity of *desma*$^{sa5-/-}$ is similar to *desma*$^{sa5+/+}$.

(C) Electron micrograph of mitochondria (M), sarcoplasmic reticulum (R), T-Tubules (T), and autophagy structures (A) in controls, *desma*$^{sa5-/-}$, and *ct122aGt* mutants. Note the sarcomeric reticulum dilatation (dR) T-tubule dilation (dT) and T-tubule bending (bT) in *desma*$^{sa5-/-}$ and the dilated mitochondria in the *ct122aGt* (dM), while these structures are normal in wild-type animals. The ratio indicates the respective frequencies (n = 6). *ct122aGt* indicates *desma*^{ct122aGt} homozygous embryos. Scale bar, 100 nm.

The error bars correspond to the SEM.

degeneration (Schröder and Schoser, 2009). In mouse, desmin knockout (KO) leads to several histological hallmarks commonly observed in desminopathy patients despite the absence of desmin aggregates. A desmin KO line *desma*$^{sa5-/-}$ was obtained from the Sanger Institute ENU-mutagenesis screen. The *desma*^{sa5} allele is a point mutation leading to a premature stop codon at the beginning of the 2B alpha helix (Figure 1H). This leads to a complete depletion of *desmin* expression as verified by *desma* mRNA quantification (Figure 1I) and further validated by western blot (Figure 1J). This suggests that the mutation leads to mRNA decay and that *desma*^{sa5} is a null allele. When analyzing the viability of the *desma*$^{sa5-/-}$, we found that *desma* depletion does not affect early embryonic overall morphology (Figure 1K); however, we noted that a significant fraction of mutants died before adult stages (25%) (Figure S2A). Similar lethality percentage was observed for the *ct122aGt* (Figure S2A).

To assess the organization of muscle fibers in the tails of embryos from both *desma*$^{sa5-/-}$ and *ct122aGt*, we used second harmonic generation (SHG) microscopy. Second harmonic light can be generated when two photons with the same frequency interact with non-centrosymmetric structures and are effectively combined to generate a new photon with twice the energy (Mojzisova and Vermot, 2011). This approach allows muscle fibers imaging without any exogenous labeling at high resolution (Plotnikov et al., 2006). From 48 hpf onward, *desma*-null embryos present perturbed organization of myofibrils with a misalignment of fibers (Figure 2A). Further investigation of *desma* loss of function was performed using two MOs, one translation blocking and one splice blocking, with a mismatch MO used as a control. Our results show that both *desma* morphants lead to similar skeletal muscle phenotypes observed for *desma*$^{sa5-/-}$ (data not shown). The same phenotype is observed in *ct122aGt* embryos from 48 hpf and is accompanied by breaks in myofibril organization in 43% of embryos at 96 hpf (n = 35) (Figure 2A). In some cases, characterized

as "extreme phenotypes," the sarcomere organization was completely lost as no SHG signal was observed (17%). The classification of our phenotype based on SHG (from weak to strong) is also correlated with the specific labeling of actin filaments in the skeletal muscle of the somite using phalloidin (Figure S3). A touch evoke assay was performed to obtain functional insight into the observed phenotypes. *ct122aGt* embryos showed a decreased swimming capacity compared to their corresponding controls with lower swimming distance and velocity, while *desma*$^{sa5-/-}$ behaved in a similar manner to *desma*$^{sa5+/+}$ (Figure 2B). The ultrastructure obtained by transmission electron microscopy (TEM) analysis of *desma*$^{sa5-/-}$ and *ct122aGt* skeletal muscles at 52 hpf (Figure 2C) showed misalignment of muscle fibers, a concomitant misalignment of T-tubules and dilatation/disorganization of the sarcoplasmic reticulum (SR), while the ER seemed unaffected in both lines. Moreover, abnormal mitochondria and mitophagy were only observed in *ct122aGt* embryos at 52 hpf. Additionally, these embryos displayed degenerating cells with loss of material and the presence of autophagosomes. Taken together, these data validate previously reported observations made in other models of desminopathies and suggest that our lines are appropriate models to study desmin function in vivo. Furthermore, our data indicate that Desmin aggregates lead to a more severe muscle phenotype than Desmin loss at the ultrastructural, cellular, and functional level.

Desma Is Required for Early Heart Function

Desmin aggregates lead to a large spectrum of phenotypes in both skeletal and cardiac muscle. The variability of phenotypes is often observed in cardiomyopathies and includes dilated, hypertrophic, and restrictive cardiomyopathy. Also in certain cases additional conduction defects are observed in adult patients (Clemen et al., 2013). Nevertheless the impact of desmin on early heart function remains unclear. Therefore, we investigate heart function in the embryo by assessing cardiac contractility using high temporal imaging of the beating heart. We found that *ct122aGt*, *ct122aRGt*, and *desma*$^{sa5-/-}$ all display an increased heart rate at 30 and 48 hpf compared to corresponding controls (Figure S4A) as well as cardiac arrhythmia (2% of the *desma*$^{sa5-/-}$ and 7% of the *ct122aGt*) (Figure S2B). We next addressed heart function by measuring the difference between diastolic and systolic chamber diameter over the corresponding diastolic diameter (also known as atrial and ventricular fractional shortening (FS%) in *desma*$^{sa5-/-}$ embryos and noted a significantly lower atrial but a significantly higher ventricular FS at 48 hpf compared to *desma*$^{sa5+/+}$. Importantly, rescue of the heart function was observed at 48 hpf in *desma*$^{sa5-/-}$ by overexpressing the zebrafish *desma* full-length mRNA, demonstrating that the abnormal heart function is specifically due to the loss of Desma in the *desma*$^{sa5-/-}$ (Figure S4A). Furthermore, *ct122aGt* and *ct122aRGt* embryos present higher atrial and lower ventricular FS at 48 hpf than the controls and the *desma* mutants. As heart dysfunction could lead to vascular defects, we measured flow velocity in the dorsal aorta of *desma*$^{sa5-/-}$, *ct122aGt*, and *ct122aRGt* embryos and found that *desma*$^{sa5-/-}$ displayed an increased arterial blood flow in contrast to *ct122aGt* and *ct122aRGt* embryos, which have lower blood flow velocities compared to controls. We also found that the blood vessel diameter was more variable than the controls, which might be associated with the somitic defects (Figures S4B–S4E). These data suggest that both desmin aggregates and levels impact wall motion in the early embryonic heart and that desminopathies can lead to early cardiac defects and abnormal vascular flow.

Heart Biomechanics Are Perturbed upon *desma* Depletion or Desmin Aggregation

To further characterize the requirement of desmin on cardiomyocyte function in vivo, we addressed the contribution of desmin to the biomechanics of the heart by monitoring key parameters defining heart-wall motion in vivo. We investigated the heart-contraction pattern in 4D in order to precisely quantify heart-wall motion during a typical heartbeat (Forouhar et al., 2006). To do so, we used the myocardial-specific *Tg(myl7:EGFP)* transgenic line. 4D reconstructions were obtained for 48 hpf *Tg(myl7:egfp) desma*$^{sa5+/+}$ (n = 5), *desma*$^{sa5-/-}$ (n = 5), and *ct122aGt* (n = 6) embryos (Figure 3A; Movies S2, S3, and S4). Quantification of the heart-wall motion in both heart chambers showed that *ct122aGt*, *ct122aRGt*, and *desma*$^{sa5-/-}$ embryos display abnormal ventricular contraction profile (Figure 3B). As the heart pumping depends on a contraction wave going from the atrium to the ventricle, we used the atrioventricular canal (AVC) displacement as a readout of the global contraction pattern. The AVC serves as a hinge, which is passively subjected to constraint due to the contraction of the atrium and ventricle. Thus, the AVC lateral motion is a mark of the synchronization between both chamber contractions (Figure 3C). To quantify the chamber synchronization, we specifically tracked the motion of the AVC cells in relation to myocardial contraction and extracted the velocity profiles of the AVC cells in the different conditions. As expected, in control embryos, the propagation of regular wave leads to a single velocity peak when the contraction wave traverses the AVC. In the absence of functional desmin (*ct122aRGt* and *desma*$^{sa5-/-}$ embryos), two velocity peaks were typically observed, demonstrating that the contraction wave does not spread uniformly along the length of the heart (Figure 3D). Together, these data show that *desma* is required to maintain proper synchronization of heart-wall motion and has an important role in coordinating the contraction wave of the heart.

Desma$^{sa5-/-}$ and *Ct122aRGt* Display Alterations in the Embryonic Heart Conduction System

It was reported that some desminopathy patients have arrhythmias associated with defects in the cardiac conduction system including calcifications (Yuri et al., 2007). Given that heart contraction waves are directly controlled by Ca^{2+} propagation in the myocardium, we tested the dynamics of Ca^{2+} propagation in our models. We used GCaMP3.0, a genetically encoded Ca^{2+} indicator (Warp et al., 2012), which reveals Ca^{2+} dynamics in the heart and the activity of the conduction system in vivo (Chi et al., 2010). We characterized the Ca^{2+} transient generation in the myocardium from *desma*$^{sa5-/-}$ and *ct122aRGt* embryos being double transgenic for *Tg(myl7:galFF)* and *Tg(UAS:GCaMP3.0)*. This permits imaging of Ca^{2+} using fast confocal microscopy and subsequent 4D reconstruction of the heartbeat and enables

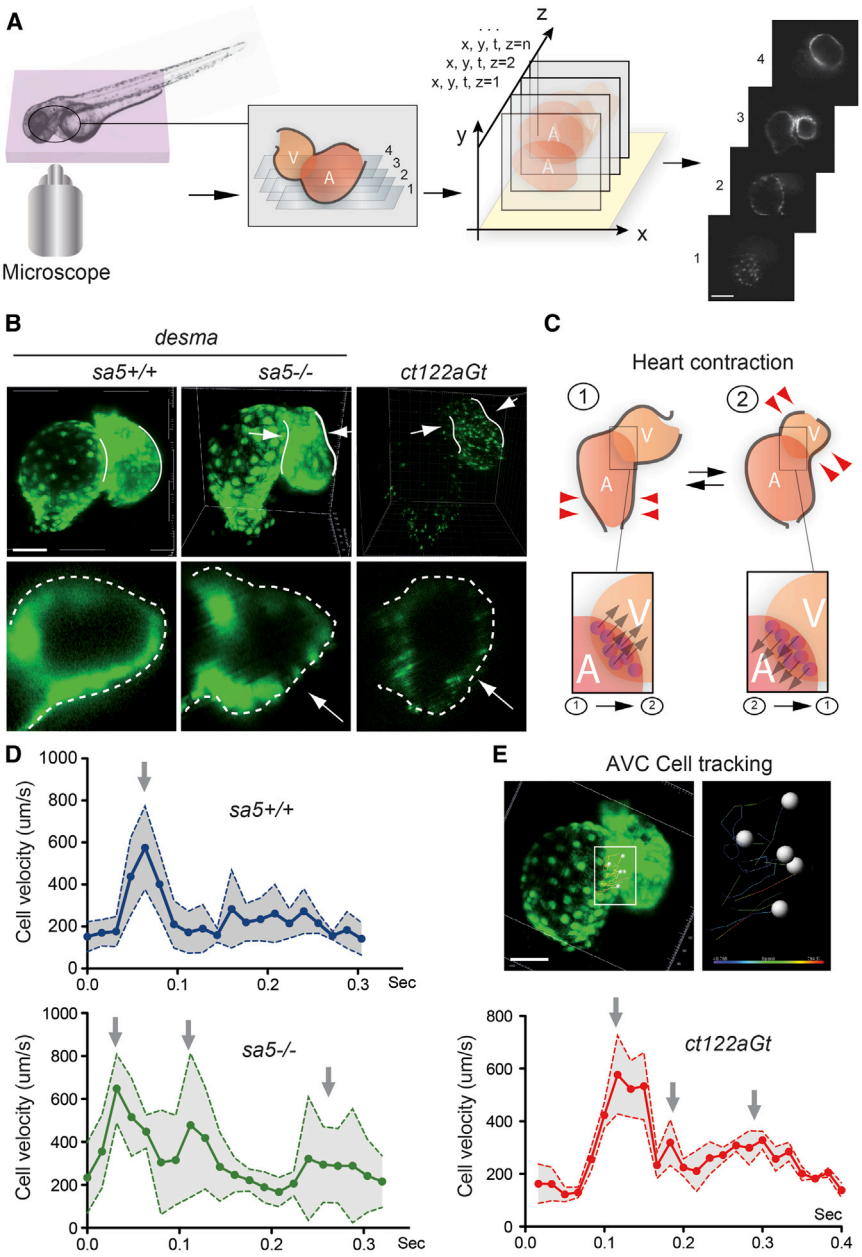

Figure 3. Heart Biomechanics Are Altered in the Absence of *desma* and in the Presence of Desmin Aggregates

(A) 4D reconstructions of the heart-wall dynamics were obtained from 2D series recorded at a rate of 120 frames/s (fps) in successive planes. Periodic contractions were reconstructed in three dimensions using post acquisition synchronization of 48-hpf embryonic hearts. Scale bar, 30 μm.

(B) Comparison of myocardial wall shape in *desma*$^{sa5+/+}$, *desma*$^{sa5-/-}$, and *ct122aGt* 4D reconstructed hearts shows a squeezing of the ventricle in both mutants (Movies S2, S3, and S4). The lower panels show a zoom of an optical transverse section through the middle of the ventricle of *desma*$^{sa5+/+}$, *desma*$^{sa5-/-}$, and *ct122aGt* revealing the squeezing in absence of functional Desma (red arrows). Scale bar, 30 μm.

(C) Schematic drawing recapitulating the myocardial movements associated with heart contraction and the subsequent movement of the atrioventricular canal (AVC). Examples of AVC cells tracks are shown in the lower panel. Their velocity was used as readout of the global contraction pattern of the heart. Scale bar, 30 μm.

(D) Graph representing the velocity of myocardial cell motion in the AVC region following 3D cell tracking in *desma*$^{sa5+/+}$, *desma*$^{sa5-/-}$, and *ct122aGt*.

(E) Individual nuclei were tracked automatically and their speed was extracted. *ct122aGt* indicates *desma*^{ct122aGt} homozygous embryos.

The error bars correspond to the SEM.

the intra-cardiac calcium fluxes to be recorded concomitantly with the native heart-wall motion (Figure 4A; Movies S5, S6, and S7). To quantify the Ca^{2+} wave, the relative fluorescence intensity was measured locally over time at the base of the atrium (1), the top of the atrium (2), the tip of the ventricle (3), and the middle of the ventricular outer curvature (4). In controls, the peaks of calcium intensity followed the contraction wave exactly and clear oscillations of fluorescence matching the contraction wave were recorded in all of the analyzed regions. By contrast, the calcium amplitude observed at the tip of the ventricle (region 3) was lower in *desma*$^{sa5-/-}$ and *ct122aRGt* embryos (1.32 ± 0.082 and 1.33 ± 0.021, respectively) compared to their corresponding controls (1.52 ± 0.082 for *desma*$^{sa5+/+}$ and 1.51 ± 0.091 for *ct122aRGt*$^{-/-}$). Similar observations were made in the region corresponding to the outer curvature of the ventricle in the *ct122aRGt* embryos (1.34 ± 0.051 compared to control 1.61 ± 0.078) (Figure 4B). These data suggest that the absence of functional desmin filaments leads to locally decreased Ca^{2+} amplitude. These observations provide the physiological basis for the aberrant contraction wave observed in the absence of functional desmin filaments as well as the abnormal synchronization between atrium and ventricle during the contraction cycles.

RyR Distribution and Localization Is Altered in *Desma*$^{sa5-/-}$ and *Ct122aRGt* Heart

Ca^{2+} flux is mostly regulated by channels that allow a fine spatio-temporal regulation of Ca^{2+} turnover. Ryanodine receptor (RyR) is a master calcium channel, which modulates the spontaneous heartbeat during development (Wu et al., 2011). Given the fact that SR shape is altered in our models, we asked whether the abnormal Ca^{2+} flux observed in our model could be linked to RyR distribution. At 48 hpf, RyR is expressed and localized on the SR membranes, while the junction of SR and T-tubules called

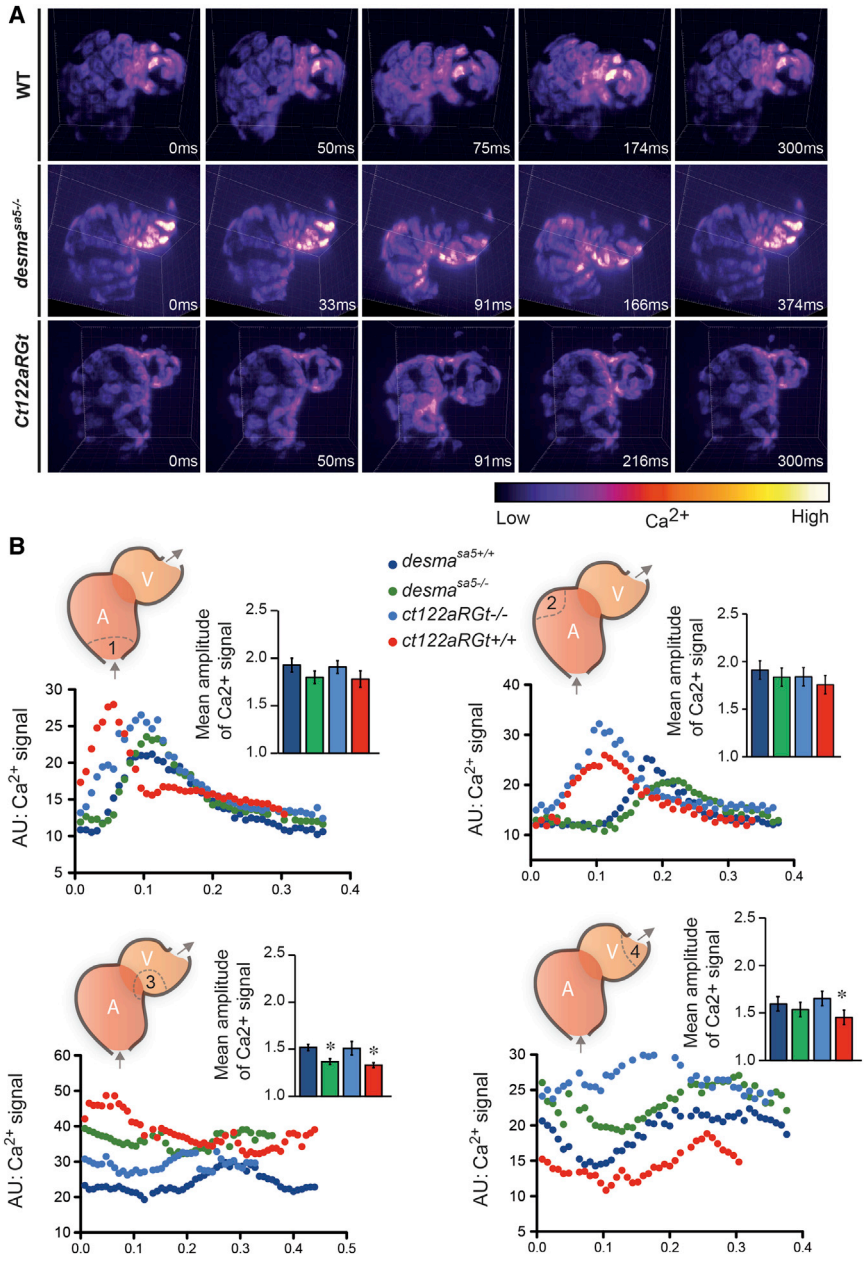

Figure 4. Ca^{2+} Propagation in the Beating Heart Is Deficient in the Absence of Functional Desmin

(A) Snapshots from videos corresponding to the 4D reconstructions of a single heartbeat in *Tg(myl7: GalFF; UAS:Gcamp3.0)* WT, *desma*$^{sa5-/-}$, and *ct122aRGt* 48-hpf embryos (Movies S5, S6, and S7) show perturbations in the Ca^{2+} signal at the ventricle tip in the absence of functional Desma. Scale bar, 30 μm.

(B) Ca^{2+} intensity plots and quantification of the amplitude of the Ca^{2+} peak upon contraction in four different regions of the heart: (1) inflow tract; (2) atrium outer curvature; (3) ventricle proximal outer curvature; and (4) ventricle distal outer curvature. The amplitude is significantly reduced in region 3 of the *desma*$^{sa5-/-}$ and in regions 3 and 4 of the *ct122aRGt* (n = 5 embryos, n ≥ 10 cells for each condition). Plots correspond to a representative example of each condition. Note that the heart-contraction sequences for each condition are not starting at the same moment of the contraction cycle. Gray arrows indicate the direction of blood flow through the heart. *ct122aRGt* indicates *desma*^{ct122aRGt} homozygous embryos. The error bars correspond to the SEM.

"the triad" (RyR localization in adult muscle) is not formed yet. However, even in the absence of mature triad compartment, RyR is expressed and functionally regulates the entry of calcium in the SR to coordinate myocardial contraction (Jurynec et al., 2008). We analyzed RyR distribution in control and in the *ct122aGt* embryos (Figure 5A). We found that RyR localization in *ct122aGt* is aberrantly accumulating and clustering in the myocardial cells (Figure 5A). We next assessed the composition of the desmin aggregates by performing solubility assay. Along with RyR, we tested for the αB-crystallin chaperone that pellets with desmin in the X100-Triton insoluble fraction (Wang et al., 2001b). We found that the insoluble (Pellet) fractions contained both αB-crystallin and RyR, along with Desmin in the *ct122aGt* embryos, while these proteins were mainly present in the soluble fractions in controls (Figure 5B). Also, we found that RyR localization and solubility were also altered in absence of Desmin in *desma*$^{sa5-/-}$ heart at 48 and 72 hpf, albeit to a lesser extent than in *ct122aGt* embryos (Figure 5C; Figures S5A and S5B). These results suggest that RyR distribution and function is affected in absence of functional desmin, which could interfere with gradual establishment of functional EC coupling machinery in muscle cells (Figure 5D).

desma Knockdown in *ct122aGt* Restores Muscle Morphology

A key step toward obtaining novel therapies of proteinopathies is the development of approaches allowing the decrease of the size and the number of aggregates. Hence, targeting desmin aggregates by decreasing *desma* level in the *ct122aGt* line will give us clues about the contribution of misfolded desmin in the muscle phenotypes. To do so, we used a MO-based approach to knockdown desmin in *ct122aGt* line. Injection of two different MO concentrations, 33 and 100 μM, lead to a drastic reduction of skeletal muscles phenotypes as assessed at 48, 72, and 96 hpf using SHG and categorized into normal (N), weak (W), strong (S), and extreme (E). We defined a scale of SHG phenotypes in which weak phenotype corresponds to the situation where muscle fibers are misaligned or present abnormal curvatures (Figure 6A). A strong phenotype is attributed when muscles display degenerated and/or broken

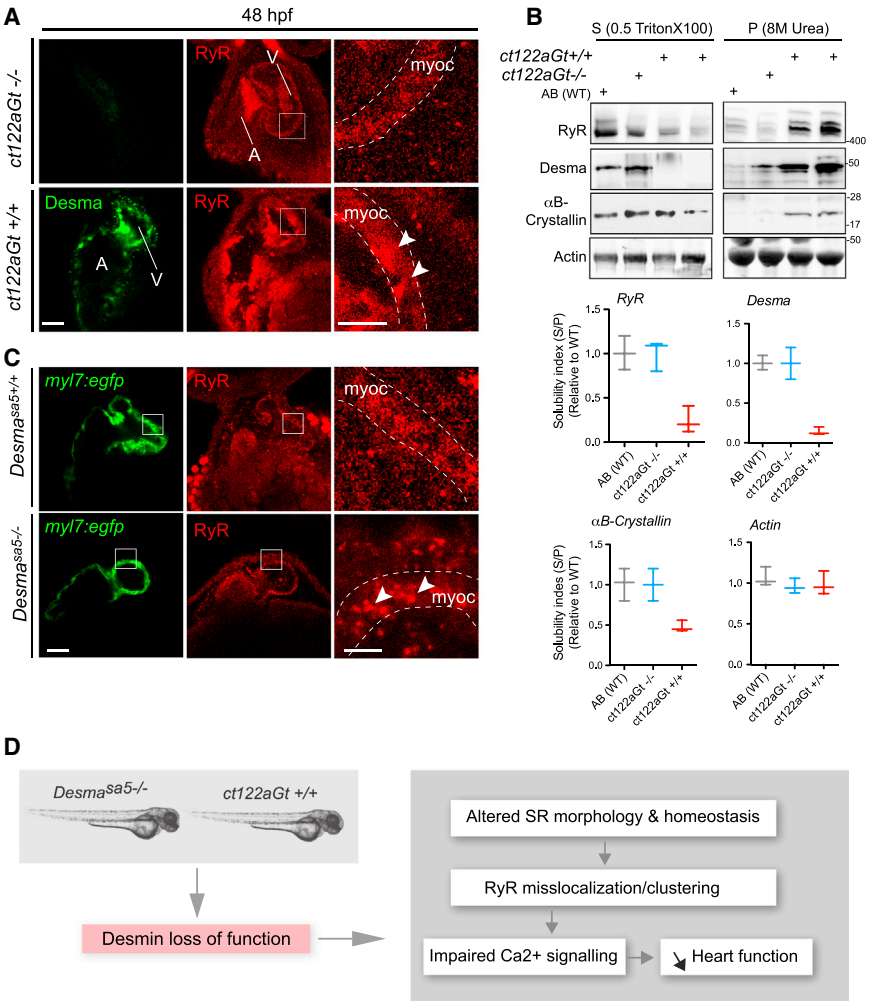

Figure 5. Desma Aggregation or Loss of Function Impact on Ryanodine Receptor Localization

(A) Confocal images of RyR (red) in cardiac muscle from 48-hpf embryos showed homogenous and regular labeling mostly in the myocardium (myoc, highlighted with the white dotted lines) in control fish (*ct122aRGt*$^{-/-}$), while in desma *ct122aRGt*$^{+/+}$ mutant hearts RyR display irregular localization and clustering (white arrowheads). Scale bar, 30 μm.

(B) In support of (A), RyR solubility was reduced in *ct122aRGt*$^{+/+}$ mutant fish extracts compared to control where the majority of RyR fraction remains in the Triton X-100 fractions. αB-crystallin solubility is also affected in *ct122aRGt*$^{+/+}$ embryos. Actin is the loading control. Bars showed quantification from two independent experiments, and each sample contains a mixture of 50–100 fish.

(C) Similar to (A), confocal images of cardiac muscle from 48-hpf embryos in *desma*$^{sa5-/-}$ animals crossed with the myocardium-specific *Tg(myl7:egfp)* (green) line compared to controls (*Tg(myl7:egfp; desma*$^{sa5+/+}$*)*) showing mislocalization and clustering (white arrowheads) of RyR in the myocardium (myoc, highlighted with the white dotted lines). Scale bar, 30 μm. myoc, myocardium

(D) Schematic drawing of how *desma* loss of function (knockout or aggregation) could impact sarcoplasmic reticulum shape and EC-coupling machinery particularly on RyR localization.

The error bars correspond to the SEM.

fibers, a global decrease in the size of the musculature or a global decrease in the intensity of the SHG signal. A phenotype is called extreme when the muscle disorganization is such that no SHG signal is observed anymore (Figure 6A). Using this scale, we found that *desma* knockdown (MO-33 and 100 μM) rescues *ct122aGt* muscle phenotypes with a complete disappearance of the strong phenotype (Figure 6B). Only weak phenotypes were observed in embryos injected with the MOs, which correlates with the drastic decrease in both the size and number of aggregates, respectively (Figure 6C). Interestingly, the effect observed is dose- dependent both in terms of aggregate size, number, and swimming distance (but not the swimming speed) and in terms of total protein decrease when additional MO concentrations were used (Figures 6D–6I). Finally the knockdown was sufficient to restore normal heart function as revealed by the rescue of the ventricular and atrial fractional shortening, whereas heart rate remained unchanged (Figure 6I). Our data show that the presence of aggregates is the main cause of pathological features in zebrafish models of desminopathies and that decreased desmin levels can reduce aggregate formation and, concomitantly, the pathology affecting the skeletal and cardiac muscles.

Doxycycline Treatment Decreases Aggregates and Ameliorates the Skeletal Muscle Phenotype in the *ct122aGt* Line

To further validate our model, we next tested compounds or drugs with the potential to act negatively on protein aggregates in the *ct122aGt* line. Doxycycline (Doxy) (Zheng et al., 2010) has raised lots of interest in the last few years and is likely the most appropriate therapeutic approach for ameliorating desminopathies. Doxy treatment lowers the aggregate content in many proteinopathies (e.g., Huntington disease) and can partially rescue the desmin-related cardiomyopathy phenotype in the αB-crystallin mouse model (Wang et al., 2001b; Zheng et al., 2010). We treated *ct122aGt* embryos with Doxy from 12 hpf and measured aggregate size and number using confocal microscopy after 36 hr of treatment (Figure 7A). We performed CLEM on Doxy-treated embryos to address the structure of the aggregates and clearance activity. The analysis revealed a more condensed and spherical structure of aggregates lacking filamentous extensions compared to vehicle-treated embryos (Figure 7A). Moreover, the size of the aggregates was found to be dramatically

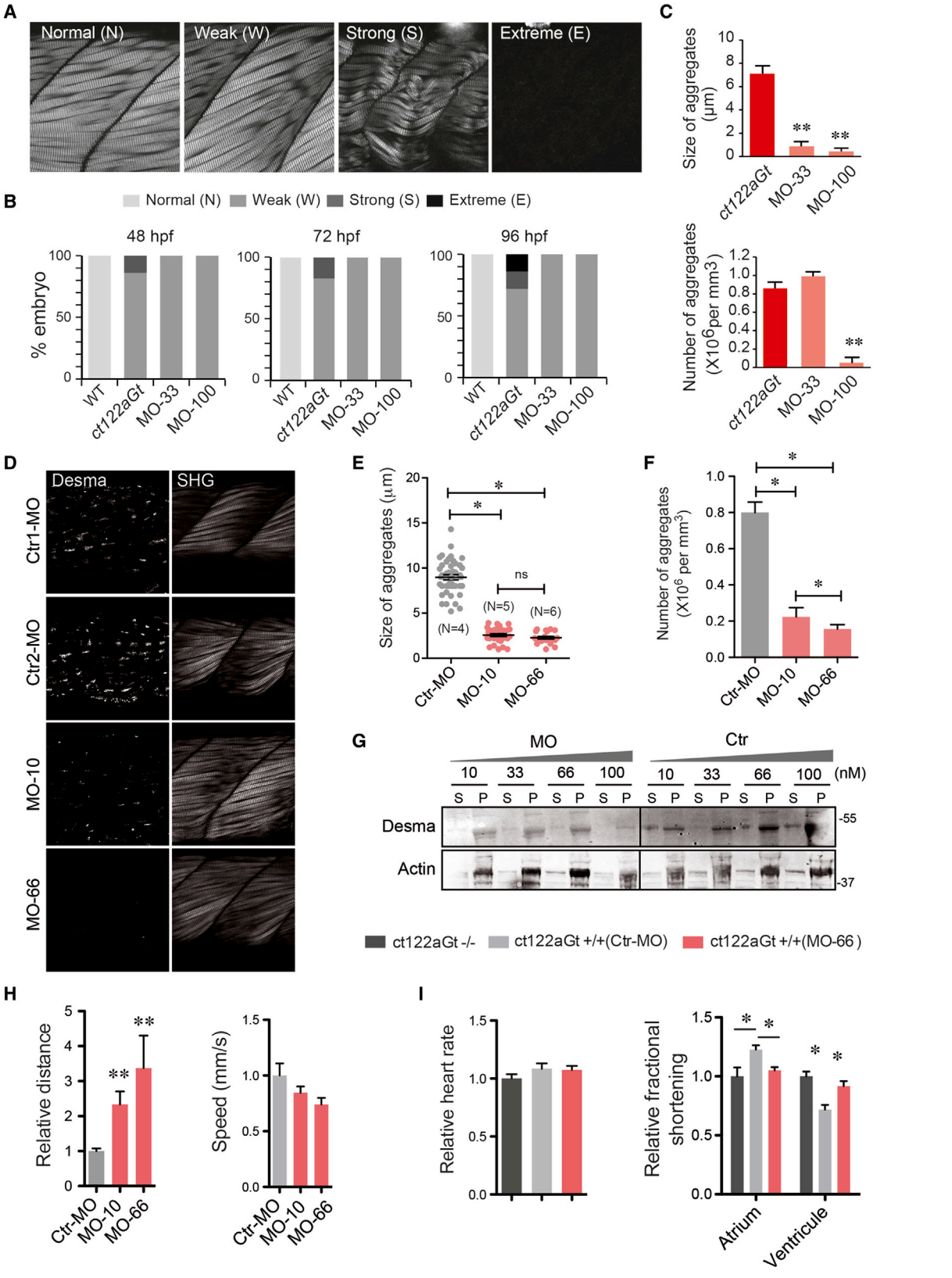

(legend on next page)

smaller in Doxy-treated embryos (3.2 ± 0.5 μm versus 9.7 ± 0.4 μm in untreated *ct122aGt*), while their number is increased (Figure 7B). We also found that Doxy-*ct122aGt* embryos displayed a weak phenotype according to our SHG analysis (100% versus 50% in corresponding controls at 72 hpf) (Figure 7C) suggesting that Doxy could fragment or/and inhibit the formation of big aggregates, which impact muscle phenotype. Doxy could also restore normal swimming distance suggesting that cellular distribution of aggregates as well as their size may have a direct impact on the severity of the phenotypes (Figure 7D). Furthermore, we found that Doxy restored normal ventricular heart rate and fractional shortening by comparison to the untreated embryos (Figure 7E). Interestingly, the atrial fractional shortening is higher in the mutants (treated and non-treated) suggesting that the rescue is heart compartment specific and that desmin affects the fractional shortening differently in the atrium and ventricle. We further addressed the impact of Doxy on desmin solubility in a dose-dependent manner. By performing solubility assays, we found that Doxy treatment dramatically increases the desmin soluble fraction comparable to that observed for controls using increased concentrations (Figure 7F). However, the beneficial impact in terms of solubility reaches a plateau when high Doxy concentration was used (50 μg/ml) (Figure 7F; Figures S6A and S6B). We also found that the effect of the Doxy could act on established aggregates as size and numbers of aggregates could also be reduced following Doxy treatment after aggregate formation (from 24 hpf) (Figure S7A). We tested Doxy activity once aggregates are formed by starting the treatment at 24 hpf and found that it still leads to a significant decrease of aggregate size and increase in their number in Doxy-*ct122aGt* lines (Figure S7B). The treated embryos developed at the same pace as controls suggesting that reduction in aggregate size is mostly due to its specific action on aggregates. We conclude that Doxy could target desmin aggregates even once they are formed and consequently could rescue muscular defects in the *ct122aGt* line. Together, these data validate the use of our line to study drugs affecting aggregate formation in vivo. It also unambiguously confirms that desmin aggregates are linked to several pathological hallmarks observed in skeletal and cardiac muscle from desminopathies.

DISCUSSION

Although the zebrafish has been used extensively to identify new regulators of cardiac and skeletal muscle function by conducting forward genetic screens, there has been very limited success in identifying novel mutants displaying aggregation phenotypes and proteinopathies using endogenously tagged proteins. By analyzing these mutant embryos, we observed the presence of aggregates when the protein is truncated or fused with fluorescent proteins. This strategy leads to aggregates that are morphologically similar to those observed in humans, unlike previous animal models in which there are no (or few) desmin aggregates (Hnia et al., 2014). Here, we took advantage of the zebrafish to analyze desmin function and desmin aggregation in the heart muscles in vivo. We found that heart defects are visible in zebrafish at embryonic stages and as the myocardium matures. The first signs of desminopathies are most frequently observed in adulthood in both mouse models and patients (Goldfarb and Dalakas, 2009). We found that embryonic heart contractility and blood flow is abnormal in the absence of desmin and in the presence of desmin aggregates in zebrafish. Desmin-null mice present arterial defects attributed to altered smooth muscle cells function where desmin is well expressed (Li et al., 1996). In the zebrafish embryo, smooth muscle cells appear at larvae stage. Considering that *desma* is not detectable in endothelial cells, our results suggest that the reported vascular phenotypes could result from an indirect impact of blood flow alterations. Although infrequent or poorly diagnosed in human desminopathies, subtle vascular abnormalities should be further investigated in relation to heart and muscle function.

The altered cardiovascular physiology observed in desmin mutants is accompanied with conduction defects leading to abnormal ventricular contraction. Remodeling of gap junctions and mislocalization of Cx43 and other mechanical junction proteins like desmoplakin, plakoglobin, and N-cadherin were shown previously in a mouse model of desmin-related cardiomyopathy (Gard et al., 2005). Mislocalization of intercellular junction components is commonly observed in arrhythmogenic cardiomyopathies and triggers a loss of mechanical and electrical coupling of cardiomyocytes (Agullo-Pascual et al., 2014; Asimaki et al., 2014). We found that distribution of RyR, an essential element

Figure 6. Reduction of Desma Level Ameliorates Skeletal and Cardiac Muscle Phenotypes Observed in *desma*^{ct122aGt} Homozygous Embryos

(A) Classification of the skeletal muscle phenotypes obtained with SHG. Normal phenotype is attributed to embryos with similar muscle shape as the controls. Weak phenotype corresponds to the situation where muscle fibers are misaligned or present abnormal curvatures. A strong phenotype is attributed when embryonic muscle display degenerated and/or broken fibers, a global decrease in the size of the musculature or a global decrease in the intensity of the SHG signal. A phenotype is called extreme when the muscle disorganization is such that no SHG signal is observed anymore. Scale bar, 30 μm.

(B) Evaluation of phenotypes in *ct122aGt* injected with the 33 and 100 μM MO, uninjected, and WT embryos from 48 to 96 hpf. The assessment of a phenotype is based on the scale presented in (A) after SHG imaging.

(C) Size and number of aggregates in *ct122aGt* injected with two different concentrations of MO (33 and 100 μM). Embryos injected with 100 μM present a high reduction in aggregate numbers, while 33 μM of MO did not reduce the aggregate number.

(D) Images of aggregates and corresponding SHG in *ct122aGt* embryos treated with 10- and 66-nM concentrations of MO or the corresponding control (Ctr). Scale bar, 30 μm.

(E and F) Two additional concentration of MO showed a dose-dependent reduction in size and number of aggregates.

(G) All the tested concentration were employed to monitor desmin solubility index = Triton X-100 soluble desmin (S)/insoluble or pellet (P) in whole zebrafish extracts. Actin is the loading control.

(H) Decreased *desma* level by MO treatment improves fish mobility but does not impact speed.

(I) MO-mediated *desma* knockdown restore normal cardiac fractional shortening in *ct122aGt* line. *ct122aGt* indicates *desma*^{ct122aGt} homozygous embryos. The error bars correspond to the SEM.

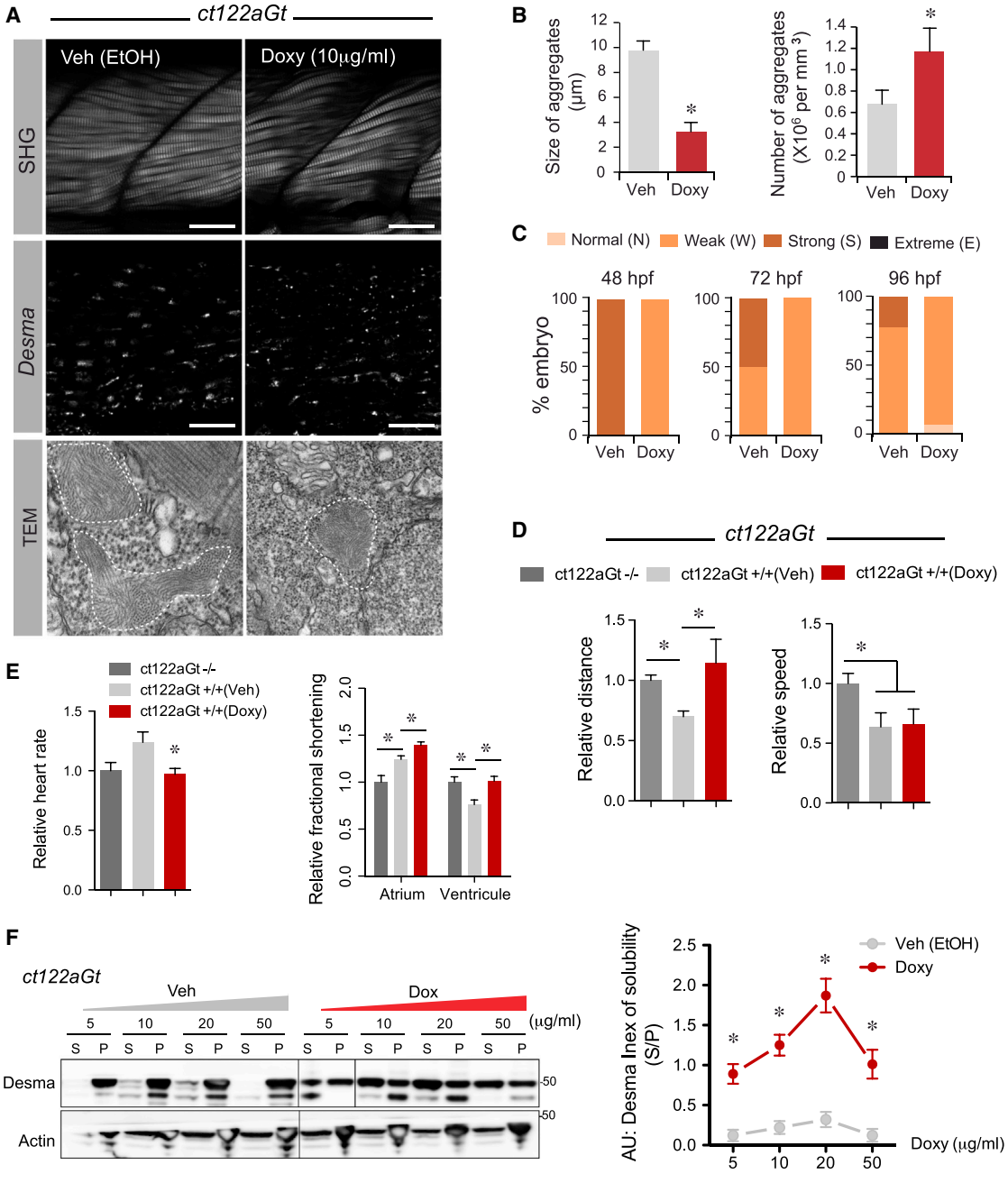

Figure 7. Pharmacological Targeting of Desma Aggregates Rescue *ct122aGt* Phenotype

(A) Confocal and electron microscopy images showing the impact of Doxycycline (Doxy) treatment on *ct122aGt* muscle. Doxy-treated embryos showed more condensed and smaller aggregates compared to the controls. Scale bar, 20 μm (SHG). Scale bar, 100 nm (TEM)

(B) Quantification of aggregate size and number in Doxy-treated embryos compared to the corresponding vehicle-treated embryos.

(C) Evaluation of the phenotypes of Doxy and vehicle-treated embryos using SHG and the scale defined in (C) show that only weak and normal phenotypes were observed after Doxy treatment, while strong phenotypes are present in the controls. Note that the vehicle contains ethanol, which is leading to a stronger phenotype than in the non-vehicle-treated *ct122aGt* line.

(D) Touch-evoke response assays showing that Doxy treatment improves swimming distance but not speed in *ct122aGt*.

(E) Doxy-treated *ct122aGt* showed increased fractional shortening (FS) in the atrium but could re-establish FS in the ventricle.

(F) Doxy treatment increases *desma* solubility (index of solubility) in dose-dependent manner. Actin is the loading control. *ct122aRGt* indicates *desma*^{ct122aRGt} homozygous embryos.

The error bars correspond to the SEM.

of the excitation contraction coupling machinery, was affected in our models. We speculate that this could explain conduction phenotypes in our models and observed in 62% of desminopathy patients (van Spaendonck-Zwarts et al., 2011). As morphogenesis of cardiomyocytes can be influenced by endogenous electrical currents in the embryonic heart (Chi et al., 2010), it is possible that desmin indirectly controls the final steps of heart development and morphogenesis through the regulation of Ca^{2+} conduction in cardiomyocytes. As our data show that the physiological mechanism of cardiac defects in desminopathies is associated with abnormal calcium dynamics in cardiomyocytes, further analysis in mouse embryos or juveniles could highlight similar features in higher vertebrates.

Finally, we employed a strategy to decrease the amount of endogenous desmin (MO) or to target the desmin aggregates (doxycycline treatment) to analyze the effects of drugs as well as to modulate the severity of the phenotype. While biochemical and cellular characterization of desmin aggregates was extremely helpful to understand properties and dynamics of these aggregates in vitro (Herrmann et al., 2009), this work should help to clarify the details of the cellular basis of desminopathies in vivo. Our data also validate the use of a knockdown strategy to decrease desmin level during early embryonic stages, which was sufficient to restore parts of the cardiac and muscular defects. Similarly, we showed that Doxy is likely acting as a chemical chaperone to interfere with existent desmin aggregates and could also inhibit gradual aggregate formation and size. We propose that future use of our desmin aggregation models *ct122aGt* and *ct122aRGt* might help to apply screening strategies for the identification of chemical compounds inhibiting desmin aggregation. As new and powerful strategies are now emerging for drug screening using whole zebrafish embryos, this will allow the potential of chemicals that could be applied in humans to be investigated. In conclusion, we have identified desmin as a potential therapeutic target for desminopathies and generated several useful zebrafish lines for modeling desminopathies.

EXPERIMENTAL PROCEDURES

Zebrafish Husbandry and Embryo Treatments

Animal experiments were approved by the Animal Experimentation Committee of the Institutional Review Board of the IGBMC. The following lines were used in this study: wild-type AB, *desma*^{ct122Gta} and *desma*^{ct122aRGt} lines (Trinh et al., 2011), *desma*^{sa5}(Kettleborough et al., 2013), *Tg(myl7:egfp)* (Huang et al., 2003), *Tg(myl7:ras-eGFP)*^{s883} (D'Amico et al., 2007), *Tg(fli1a:neGFP)*^{y7} (Roman et al., 2002), *Tg(fli:gal4FF*^{ubs}*; UAS:kaede)* (Herwig et al., 2011), *Tg(myl7:GalFF; UAS:RFP)*^{hu6228} (Strate et al., 2015), and *Tg(UAS:gcamp3.0; Gal4s1020t)* (Warp et al., 2012) and were described previously. Embryos were staged according to hours (hpf) and days postfertilization (dpf). They were incubated at 28.5°C in 0.3% Danieau medium supplemented with 0.003% (w/v) 2-phenylthiourea to inhibit pigment formation.

desma^{sa5} fish were genotyped using the following primers: FP: ACACA CACTCGCCAAACAAA and RP: GTCTCAGCAACTTCCGGTTC. For imaging, embryos were anesthetized with 0.02% Tricaine (Sigma-Aldrich) and were mounted on glass bottom Petri dishes embedded in 0.8% low melting point agarose (Sigma-Aldrich). Before fixation for electron microscopy and still heart imaging, embryos were treated for 10 min with 40 mM 2,3-butanedione monoxime (BDM) as a myosin inhibitor to have their muscle in a constant relaxed state. Doxycycline (Sigma-Aldrich) was supplemented in the fish medium from 12 hpf at 10 μg/ml.

Morpholino Knockdown and mRNA Rescue

One translation start site blocking and one splice site blocking MO were designed to knockdown *desma* (Gene Tools). *desma* ATG MO: GGCTGAAT ATTTCGTGCTCATGACT, *desma* splice MO (exon 2-intron 2): ATGACATAA AGTACATACAGCTCTG. *desma* ATG mismatched MO (GGCTCAAAATT TGGTCCTCATCACT) was used as control. 2.3 nl of MO (100 μM) was injected into embryos at one-cell stage. For rescue experiments in *desma*$^{sa5-/-}$, full-length zebrafish *desma* cDNA was obtained in pME18SFL3 (Source Bioscience) and amplified using TAATACGACTCACTATAGGGACCATGAGCACGA AATATTCAGC and GGATCCAGACATGATAAGATAC primers. The resulting fragments were transcribed in vitro using mMessage mMachine T7 Kit (Ambion). 0.25 ng of the mRNA was injected into embryos at the one-cell stage.

SUPPLEMENTAL INFORMATION

Supplemental Information includes Supplemental Experimental Procedures, seven figures, and seven movies and can be found with this article online at http://dx.doi.org/10.1016/j.celrep.2015.05.010.

ACKNOWLEDGMENTS

We thank D. Paulin for thoughtful comments on the manuscript. We thank S. Abdelilah-Seyfried, M. Affolter, and C. Wyart for providing fish stocks. We thank the IGBMC fish facility (S. Geschier and S. Gredler) and the IGBMC imaging center, in particular B. Gurchenkov, P. Kessler, M. Koch, and D. Hentsch. This work was supported by HFSP, INSERM, AFM, FRM, and the seventh framework program (MC-IRG256549 to J.V.). C.R. was supported by the AFM. This study was supported by grant ANR-10-LABX-0030-INRT, a French State fund managed by the Agence Nationale de la Recherche under the frame program Investissements d'Avenir labeled ANR-10-IDEX-0002-02.

Received: July 25, 2014
Revised: April 3, 2015
Accepted: May 5, 2015
Published: June 4, 2015

REFERENCES

Agullo-Pascual, E., Cerrone, M., and Delmar, M. (2014). Arrhythmogenic cardiomyopathy and Brugada syndrome: diseases of the connexome. FEBS Lett. *588*, 1322–1330.

Anderson, J., Li, Z., and Goubel, F. (2001). Passive stiffness is increased in soleus muscle of desmin knockout mouse. Muscle Nerve *24*, 1090–1092.

Asimaki, A., Kapoor, S., Plovie, E., Karin Arndt, A., Adams, E., Liu, Z., James, C.A., Judge, D.P., Calkins, H., Churko, J., et al. (2014). Identification of a new modulator of the intercalated disc in a zebrafish model of arrhythmogenic cardiomyopathy. Sci. Transl. Med. *6*, 40ra74.

Balogh, J., Merisckay, M., Li, Z., Paulin, D., and Arner, A. (2002). Hearts from mice lacking desmin have a myopathy with impaired active force generation and unaltered wall compliance. Cardiovasc. Res. *53*, 439–450.

Bär, H., Fischer, D., Goudeau, B., Kley, R.A., Clemen, C.S., Vicart, P., Herrmann, H., Vorgerd, M., and Schröder, R. (2005a). Pathogenic effects of a novel heterozygous R350P desmin mutation on the assembly of desmin intermediate filaments in vivo and in vitro. Hum. Mol. Genet. *14*, 1251–1260.

Bär, H., Mücke, N., Kostareva, A., Sjöberg, G., Aebi, U., and Herrmann, H. (2005b). Severe muscle disease-causing desmin mutations interfere with in vitro filament assembly at distinct stages. Proc. Natl. Acad. Sci. USA *102*, 15099–15104.

Bär, H., Schopferer, M., Sharma, S., Hochstein, B., Mücke, N., Herrmann, H., and Willenbacher, N. (2010). Mutations in desmin's carboxy-terminal "tail" domain severely modify filament and network mechanics. J. Mol. Biol. *397*, 1188–1198.

Brodehl, A., Hedde, P.N., Dieding, M., Fatima, A., Walhorn, V., Gayda, S., Šarić, T., Klauke, B., Gummert, J., Anselmetti, D., et al. (2012). Dual color photoactivation localization microscopy of cardiomyopathy-associated desmin mutants. J. Biol. Chem. *287*, 16047–16057.

Chi, N.C., Bussen, M., Brand-Arzamendi, K., Ding, C., Olgin, J.E., Shaw, R.M., Martin, G.R., and Stainier, D.Y. (2010). Cardiac conduction is required to preserve cardiac chamber morphology. Proc. Natl. Acad. Sci. USA *107*, 14662–14667.

Clemen, C.S., Herrmann, H., Strelkov, S.V., and Schröder, R. (2013). Desminopathies: pathology and mechanisms. Acta Neuropathol. *125*, 47–75.

Costa, M.L., Escaleira, R., Cataldo, A., Oliveira, F., and Mermelstein, C.S. (2004). Desmin: molecular interactions and putative functions of the muscle intermediate filament protein. Braz. J. Med. Biol. Res. *37*, 1819–1830.

D'Amico, L., Scott, I.C., Jungblut, B., and Stainier, D.Y. (2007). A mutation in zebrafish hmgcr1b reveals a role for isoprenoids in vertebrate heart-tube formation. Curr. Biol. *17*, 252–259.

Forouhar, A.S., Liebling, M., Hickerson, A., Nasiraei-Moghaddam, A., Tsai, H.J., Hove, J.R., Fraser, S.E., Dickinson, M.E., and Gharib, M. (2006). The embryonic vertebrate heart tube is a dynamic suction pump. Science *312*, 751–753.

Gard, J.J., Yamada, K., Green, K.G., Eloff, B.C., Rosenbaum, D.S., Wang, X., Robbins, J., Schuessler, R.B., Yamada, K.A., and Saffitz, J.E. (2005). Remodeling of gap junctions and slow conduction in a mouse model of desmin-related cardiomyopathy. Cardiovasc. Res. *67*, 539–547.

Goldfarb, L.G., and Dalakas, M.C. (2009). Tragedy in a heartbeat: malfunctioning desmin causes skeletal and cardiac muscle disease. J. Clin. Invest. *119*, 1806–1813.

Griggs, R., Vihola, A., Hackman, P., Talvinen, K., Haravuori, H., Faulkner, G., Eymard, B., Richard, I., Selcen, D., Engel, A., et al. (2007). Zaspopathy in a large classic late-onset distal myopathy family. Brain *130*, 1477–1484.

Herrmann, H., Strelkov, S.V., Burkhard, P., and Aebi, U. (2009). Intermediate filaments: primary determinants of cell architecture and plasticity. J. Clin. Invest. *119*, 1772–1783.

Herwig, L., Blum, Y., Krudewig, A., Ellertsdottir, E., Lenard, A., Belting, H.G., and Affolter, M. (2011). Distinct cellular mechanisms of blood vessel fusion in the zebrafish embryo. Curr. Biol. *21*, 1942–1948.

Hnia, K., Tronchere, H., Tomczak, K.K., Amoasii, L., Schultz, P., Beggs, A.H., Payrastre, B., Mandel, J.L., and Laporte, J. (2011). Myotubularin controls desmin intermediate filament architecture and mitochondrial dynamics in human and mouse skeletal muscle. The Journal of clinical investigation *121*, 70–85.

Hnia, K., Ramspacher, C., Vermot, J., and Laporte, J. (2014). Desmin in muscle and associated diseases: beyond the structural function. Cell Tissue Res.

Huang, C.J., Tu, C.T., Hsiao, C.D., Hsieh, F.J., and Tsai, H.J. (2003). Germ-line transmission of a myocardium-specific GFP transgene reveals critical regulatory elements in the cardiac myosin light chain 2 promoter of zebrafish. Dev. Dyn. *228*, 30–40.

Joanne, P., Chourbagi, O., Hourdé, C., Ferry, A., Butler-Browne, G., Vicart, P., Dumonceaux, J., and Agbulut, O. (2013). Viral-mediated expression of desmin mutants to create mouse models of myofibrillar myopathy. Skelet Muscle *3*, 4.

Jurynec, M.J., Xia, R., Mackrill, J.J., Gunther, D., Crawford, T., Flanigan, K.M., Abramson, J.J., Howard, M.T., and Grunwald, D.J. (2008). Selenoprotein N is required for ryanodine receptor calcium release channel activity in human and zebrafish muscle. Proc. Natl. Acad. Sci. USA *105*, 12485–12490.

Kettleborough, R.N., Busch-Nentwich, E.M., Harvey, S.A., Dooley, C.M., de Bruijn, E., van Eeden, F., Sealy, I., White, R.J., Herd, C., Nijman, I.J., et al. (2013). A systematic genome-wide analysis of zebrafish protein-coding gene function. Nature *496*, 494–497.

Kostareva, A., Sjöberg, G., Bruton, J., Zhang, S.J., Balogh, J., Gudkova, A., Hedberg, B., Edström, L., Westerblad, H., and Sejersen, T. (2008). Mice expressing L345P mutant desmin exhibit morphological and functional changes of skeletal and cardiac mitochondria. J. Muscle Res. Cell Motil. *29*, 25–36.

Lacolley, P., Challande, P., Boumaza, S., Cohuet, G., Laurent, S., Boutouyrie, P., Grimaud, J.A., Paulin, D., Lamazière, J.M., and Li, Z. (2001). Mechanical properties and structure of carotid arteries in mice lacking desmin. Cardiovasc. Res. *51*, 178–187.

Li, Z., Colucci-Guyon, E., Pinçon-Raymond, M., Mericskay, M., Pournin, S., Paulin, D., and Babinet, C. (1996). Cardiovascular lesions and skeletal myopathy in mice lacking desmin. Dev. Biol. *175*, 362–366.

Li, M., Andersson-Lendahl, M., Sejersen, T., and Arner, A. (2013). Knockdown of desmin in zebrafish larvae affects interfilament spacing and mechanical properties of skeletal muscle. J. Gen. Physiol. *141*, 335–345.

Milner, D.J., Weitzer, G., Tran, D., Bradley, A., and Capetanaki, Y. (1996). Disruption of muscle architecture and myocardial degeneration in mice lacking desmin. J. Cell Biol. *134*, 1255–1270.

Mojzisova, H., and Vermot, J. (2011). When multiphoton microscopy sees near infrared. Curr. Opin. Genet. Dev. *21*, 549–557.

Plotnikov, S.V., Millard, A.C., Campagnola, P.J., and Mohler, W.A. (2006). Characterization of the myosin-based source for second-harmonic generation from muscle sarcomeres. Biophys. J. *90*, 693–703.

Raats, J.M., Schaart, G., Henderik, J.B., van der Kemp, A., Dunia, I., Benedetti, E.L., Pieper, F.R., Ramaekers, F.C., and Bloemendal, H. (1996). Muscle-specific expression of a dominant negative desmin mutant in transgenic mice. Eur. J. Cell Biol. *71*, 221–236.

Rezniczek, G.A., Konieczny, P., Nikolic, B., Reipert, S., Schneller, D., Abrahamsberg, C., Davies, K.E., Winder, S.J., and Wiche, G. (2007). Plectin 1f scaffolding at the sarcolemma of dystrophic (mdx) muscle fibers through multiple interactions with beta-dystroglycan. J. Cell Biol. *176*, 965–977.

Roman, B.L., Pham, V.N., Lawson, N.D., Kulik, M., Childs, S., Lekven, A.C., Garrity, D.M., Moon, R.T., Fishman, M.C., Lechleider, R.J., and Weinstein, B.M. (2002). Disruption of acvrl1 increases endothelial cell number in zebrafish cranial vessels. Development *129*, 3009–3019.

Schröder, R., and Schoser, B. (2009). Myofibrillar myopathies: a clinical and myopathological guide. Brain Pathol. *19*, 483–492.

Shardonofsky, F.R., Capetanaki, Y., and Boriek, A.M. (2006). Desmin modulates lung elastic recoil and airway responsiveness. Am. J. Physiol. Lung Cell. Mol. Physiol. *290*, L890–L896.

Strate, I., Tessadori, F., and Bakkers, J. (2015). Glypican4 promotes cardiac specification and differentiation by attenuating canonical Wnt and Bmp signaling. Development *142*, 1767–1776.

Trinh, A., Hochgreb, T., Graham, M., Wu, D., Ruf-Zamojski, F., Jayasena, C.S., Saxena, A., Hawk, R., Gonzalez-Serricchio, A., Dixson, A., et al. (2011). A versatile gene trap to visualize and interrogate the function of the vertebrate proteome. Genes Dev. *25*, 2306–2320.

van Spaendonck-Zwarts, K.Y., van Hessem, L., Jongbloed, J.D., de Walle, H.E., Capetanaki, Y., van der Kooi, A.J., van Langen, I.M., van den Berg, M.P., and van Tintelen, J.P. (2011). Desmin-related myopathy. Clin. Genet. *80*, 354–366.

Vogel, B., Meder, B., Just, S., Laufer, C., Berger, I., Weber, S., Katus, H.A., and Rottbauer, W. (2009). In-vivo characterization of human dilated cardiomyopathy genes in zebrafish. Biochem. Biophys. Res. Commun. *390*, 516–522.

Wang, X., Osinska, H., Dorn, G.W., 2nd, Nieman, M., Lorenz, J.N., Gerdes, A.M., Witt, S., Kimball, T., Gulick, J., and Robbins, J. (2001a). Mouse model of desmin-related cardiomyopathy. Circulation *103*, 2402–2407.

Wang, X., Osinska, H., Klevitsky, R., Gerdes, A.M., Nieman, M., Lorenz, J., Hewett, T., and Robbins, J. (2001b). Expression of R120G-alphaB-crystallin causes aberrant desmin and alphaB-crystallin aggregation and cardiomyopathy in mice. Circ. Res. *89*, 84–91.

Warp, E., Agarwal, G., Wyart, C., Friedmann, D., Oldfield, C.S., Conner, A., Del Bene, F., Arrenberg, A.B., Baier, H., and Isacoff, E.Y. (2012). Emergence of patterned activity in the developing zebrafish spinal cord. Curr. Biol. *22*, 93–102.

Wu, H.H., Brennan, C., and Ashworth, R. (2011). Ryanodine receptors, a family of intracellular calcium ion channels, are expressed throughout early vertebrate development. BMC Res. Notes *4*, 541.

Yuri, T., Miki, K., Tsukamoto, R., Shinde, A., Kusaka, H., and Tsubura, A. (2007). Autopsy case of desminopathy involving skeletal and cardiac muscle. Pathol. Int. *57*, 32–36.

Zheng, H., Tang, M., Zheng, Q., Kumarapeli, A.R., Horak, K.M., Tian, Z., and Wang, X. (2010). Doxycycline attenuates protein aggregation in cardiomyocytes and improves survival of a mouse model of cardiac proteinopathy. J. Am. Coll. Cardiol. *56*, 1418–1426.